RESEARCH ARTICLE

Weathering above the tides: how iceberg-roll-generated waves shape Arctic rocky shores

Oskar Kostrzewa, Małgorzata Szczypińska, Krzysztof Senderak & Mateusz C. Strzelecki
Alfred Jahn Cold Regions Research Centre, Institute of Geography and Regional Development, University of Wrocław, Wrocław, Poland

Abstract

A significant limitation of the current understanding of cold coast evolution is the paucity of field observations on the development of rocky coasts in glaciated parts of the Arctic. To address this gap, we present a pilot study that utilizes a Schmidt hammer to investigate variations in rock surface resistance across four distinct horizontal zones along the rocky bay of Zion Church, Ilulissat, near one of the prevailing routes of iceberg transport in western Greenland. The primary finding of the study is a substantial decrease in rock resistance within the area above the high-tide level. We relate this result mainly to waves generated by iceberg-roll events in conjunction with chemical and biological weathering. This case study seeks to elevate the status of iceberg-roll-generated waves from a mere curiosity to a substantial geomorphic agent that shapes the microrelief of Arctic coastlines.

Keywords

West Greenland; rocky coasts; Schmidt hammer; iceberg-capsize tsunamis; glacier-calving tsunamis

Correspondence

Oskar Kostrzewa, Alfred Jahn Cold Regions Research Centre, Institute of Geography and Regional Development, University of Wrocław, pl. Uniwersytecki 1, 50-137 Wrocław, Poland. E-mail: oskar.kostrzewa@uwr.edu.pl

Introduction

The morphology of Arctic coasts is subject to dynamic changes driven by marine and atmospheric processes, as well as the degradation of the cryosphere. These coasts comprise both lithified and unlithified sections, with erosion rates largely dependent on local lithological and climatic conditions (Irrgang et al. 2022). However, there is still a lack of detailed process-based studies on the coastal development of glaciated areas such as Greenland, Svalbard and the Canadian Arctic Archipelago, compared to the more extensively studied sedimentary coasts of Siberia and Alaska.

To date, research in these paraglacial settings has often focused on the dynamics of coasts fed by large sediment pulses from glacial rivers, which can form new beaches, barriers, spits and deltas (e.g., Bendixen et al. 2017; Strzelecki et al. 2018; Zagórski et al. 2020; Kavan & Strzelecki 2023). However, this focus on sedimentary systems overlooks another critical outcome of deglaciation: the exposure of new stretches of rocky coastline.

Although 35% of the Arctic coast is formed in rocky terrain (Lantuit et al. 2012), until fairly recently, few studies concentrated on mechanisms shaping their geomorphology. Lately, a number of studies focusing on coastal erosion and weathering patterns have addressed this knowledge gap (e.g., Strzelecki 2017; Strzelecki et al. 2017; Lim et al. 2020; Aga et al. 2024). The range of processes responsible for shaping Arctic rocky coasts was summarized by Strzelecki et al. (2017) on the basis of several years of research on Svalbard rocky coast environments. The evolution of such coasts is controlled by postglacial rock uplift and relative changes in sea level (e.g., Forman et al. 2004), seasonal sea-ice activity, frost weathering (e.g., Shakesby & Matthews 1987), icefoot activity (e.g., Nielsen 1979), permafrost-dependent rock saturation (e.g., Kasprzak et al. 2017), snow isolation (e.g., Trenhaile & Mercan 1984; Dawson et al. 1987) and the influence of biogenic forcings (e.g., Strzelecki 2017).

Here, we would like to complement the picture of factors with tsunami-like waves associated with cryospheric degradation (Fig. 1). Glaciated regions of the Arctic are also often characterized by microtides and reduced storm wave action attributed to constraining fjord topography and sea-ice cover, especially in colder months (Strzelecki et al. 2017). This is very important because the waves associated with cryospheric degradation in some particular locations may be the only type of wave action able to strongly modify coastal morphology (Kostrzewa et al. 2024). The waves associated with glacier calving or iceberg roll can occur daily in some places during the Arctic summer (e.g., Long et al. 2015), leading to morphological

Citation: *Polar Research* 2026, *45*, 12395, http://dx.doi.org/10.33265/polar.v45.12395

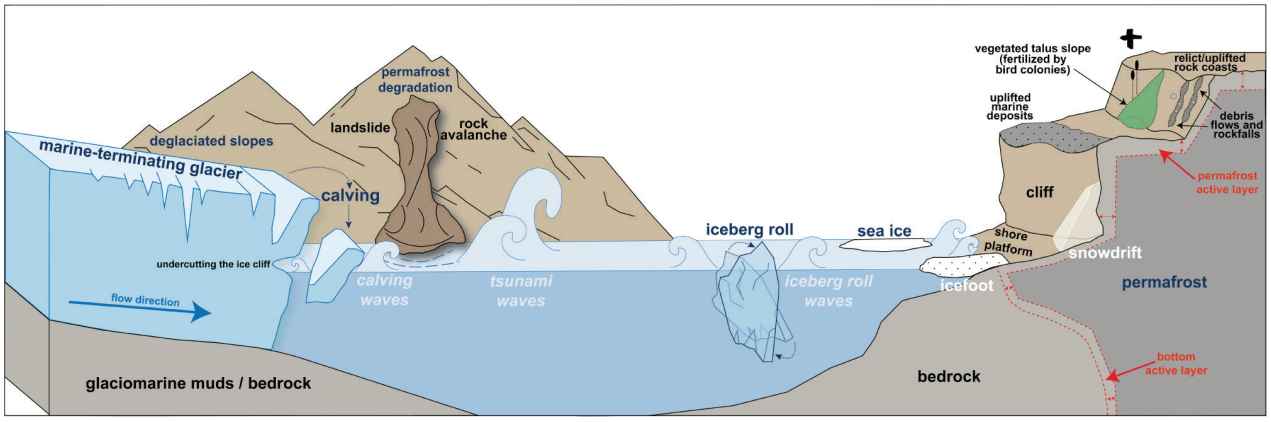

Fig. 1 Conceptual model of factors shaping rocky coasts in glaciated regions of the Arctic, modified from Strzelecki et al. (2017). Note that apart from standard cryo-conditioned factors such as sea ice, snow, permafrost and periglacial processes, the morphology of rocky shores may be modified by the impact of extreme waves triggered by landslides, glacier calving or iceberg-roll events, as presented in this study.

transformations in a short period of time. At the same time, waves contribute to an extremely efficient mechanical weathering process: wet–dry and freeze–thaw cycles. A recent study indicates that a calving wave is capable of entraining boulders more than 1 m in diameter and transporting them over distances of up to 3 m (Kostrzewa et al. 2024). An extreme wave that transforms the coast not only redistributes boulders and fine sediments but can also detach fragments of cracked rock outcrops (Kostrzewa et al. 2024). Observations in Alaska (Higman et al. 2018), west Greenland (Buchwał et al. 2015; Strzelecki & Jaskólski 2020; Svennevig et al. 2023) and east Greenland (Svennevig et al. 2024) have shown that the unstable nature of deglaciated slopes along the narrow and steep coasts of Arctic fjords may potentially provide favourable conditions for landslides and rockfalls, which can trigger tsunami waves. In addition, Strzelecki & Jaskólski (2020) demonstrated the morphogenetic power of an Arctic tsunami, which was capable of eroding the top of coastal cliffs and transporting boulders from local beaches more than 100 m inland. Extreme waves caused by landslides, glacier calving and iceberg-roll events are predicted to increase in a warmer future characterized by destabilized and deglacierized Arctic shores, and their influence on coastal geomorphology requires further study. This rapid transition from a subglacial to a paraglacial rocky landscape, and the specific weathering processes at play, represent a significant knowledge gap that this paper aims to address.

The recession of marine-terminating glaciers not only feeds accumulation coasts but also creates new environments on rocky coasts where the rocks ploughed by glaciers form new cliffs and shore platforms (Fig. 1; Strzelecki et al. 2017; Strzelecki et al. 2020). In addition, areas near marine-terminating glaciers are subject to the impact of waves induced by glacier calving (e.g., Nielsen 1992; Kostrzewa et al. 2024, Fig. 2). Kostrzewa et al. (2024) further illustrated this by showing that a single wave caused by glacial calving rebuilt the local beaches and that, over the years, calving waves led to the lagoon's closure from the bay. It has been suggested that glacial calving waves are similar to tsunamis caused by landslides and earthquakes, though they are smaller in size and no full water column movement is observed during their formation (Wolper et al. 2021). There is an additional tsunami risk from the unstable nature of deglaciated slopes along narrow and steep coasts of Arctic fjords, which may provide favourable conditions for landslides and rockfalls (Fig. 2).

Another type of wave clearly related to cryospheric processes is the iceberg-roll-generated wave observed in the natural conditions during the transport of broken parts of the glacier in Arctic waters. As a drifting iceberg melts, its centre of gravity shifts and it rocks and rotates to reach a new equilibrium, producing waves that typically reach heights of up to 2 m at the point of generation (Amundson et al. 2008; MacAyeal et al. 2009). According to MacAyeal et al. (2011), the initial deep-water wave height is approximately 100th of the iceberg's thickness, although the resulting breaking wave height and period may vary depending on local bathymetry and shoreline configuration. Despite the preservation of iceberg-roll events in the sediments of isolation basins along the southern coast of Disko Bay, Greenland (Fig. 2; Long et al. 2015), the impact of these waves on Arctic coastal morphodynamics has not been thoroughly investigated.

Given the regular occurrence of waves caused by iceberg-roll events around Jakobshavn Isfjord in Greenland, we examined whether these effects could be detected in the microrelief of predominantly rocky bays. To date, the effects of extreme waves in glacial environments,

Citation: *Polar Research* 2026, *45*, 12395, http://dx.doi.org/10.33265/polar.v45.12395

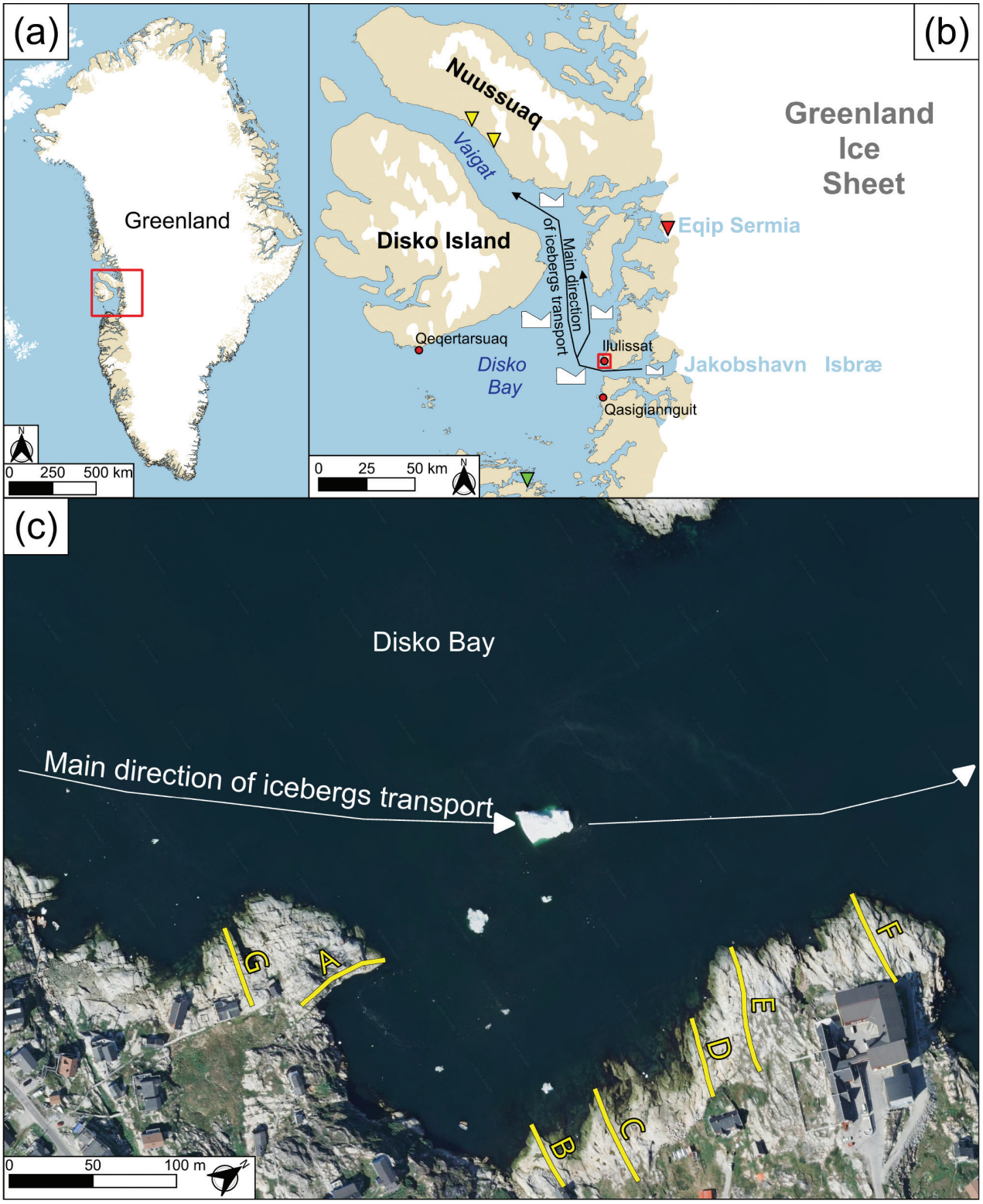

Fig. 2 (a) The location of Disko Bay in Greenland. (b) The main direction of iceberg transport (black arrows) in Disko Bay and location of previous studies on wave impact on coastal zones: landslide tsunamis (yellow triangles; Buchwał et al. 2015; Svennevig et al. 2023); calving waves (red triangle; Kostrzewa et al. 2024); iceberg-roll waves (green triangle; Long et al. 2015). (c) The seven profiles in Zion Church Bay along which measurements were made (background map: Google Maps).

such as landslide-triggered tsunamis, calving waves and iceberg-roll-generated waves, have not been incorporated into conceptual models of cryo-conditioned rocky coasts (Strzelecki et al. 2017). This motivated us to conduct observations along shores that had experienced at least one of these extreme wave events.

In this pilot study, Schmidt hammer rock tests were utilized to characterize the degree of weathering of rocky shorelines and to determine whether an area inundated by iceberg-roll waves exhibited distinctive characteristics compared to a shoreline inundated by tides and an upper shore zone that had become isolated from the sea and partially vegetated. The measurements were carried out on Archaean grey tonalitic orthogneiss, a crystalline rock that is widespread near Ilulissat (Garde et al. 2002).

Study area

The study was carried out in Zion Church Bay, one of the rocky bays of Disko Bay, in Ilulissat, west Greenland (Figs. 2, 3). Icebergs from the glacier Jakobshavn Isbræ almost entirely fill the fjord throughout the year (Fig. 2). This greatly dampens the impact of storm waves, especially between December/January and May/June, when there is nearshore sea ice and an icefoot complex (Ribeiro et al. 2012; Møller et al. 2023). Storm waves developing in Davis Strait are diffracted by the "icy breakwaters" formed by icebergs and sea ice, which can reduce wave energy and alter wave propagation patterns (Bendixen & Kroon 2017). Presumably, the primary type of wave that exceeds the 2-m tidal range (Dietrich et al. 2007) and runs up the furthest beyond the high-water mark is that generated by iceberg-roll events. The testing area is approximately 2 km north of the mouth of Jakobshavn Isfjord (Fig. 2). As the fastest-moving glacier in the world (Joughin et al. 2004), Jakobshavn Isbræ (69°10′N, 50°00′W) is the subject of considerable research. Icebergs that calve from this glacier drift into Disko Bay, where they may roll over. As they approach Ilulissat, these rolling events can generate waves that impact the rocky coastline. While some of the icebergs

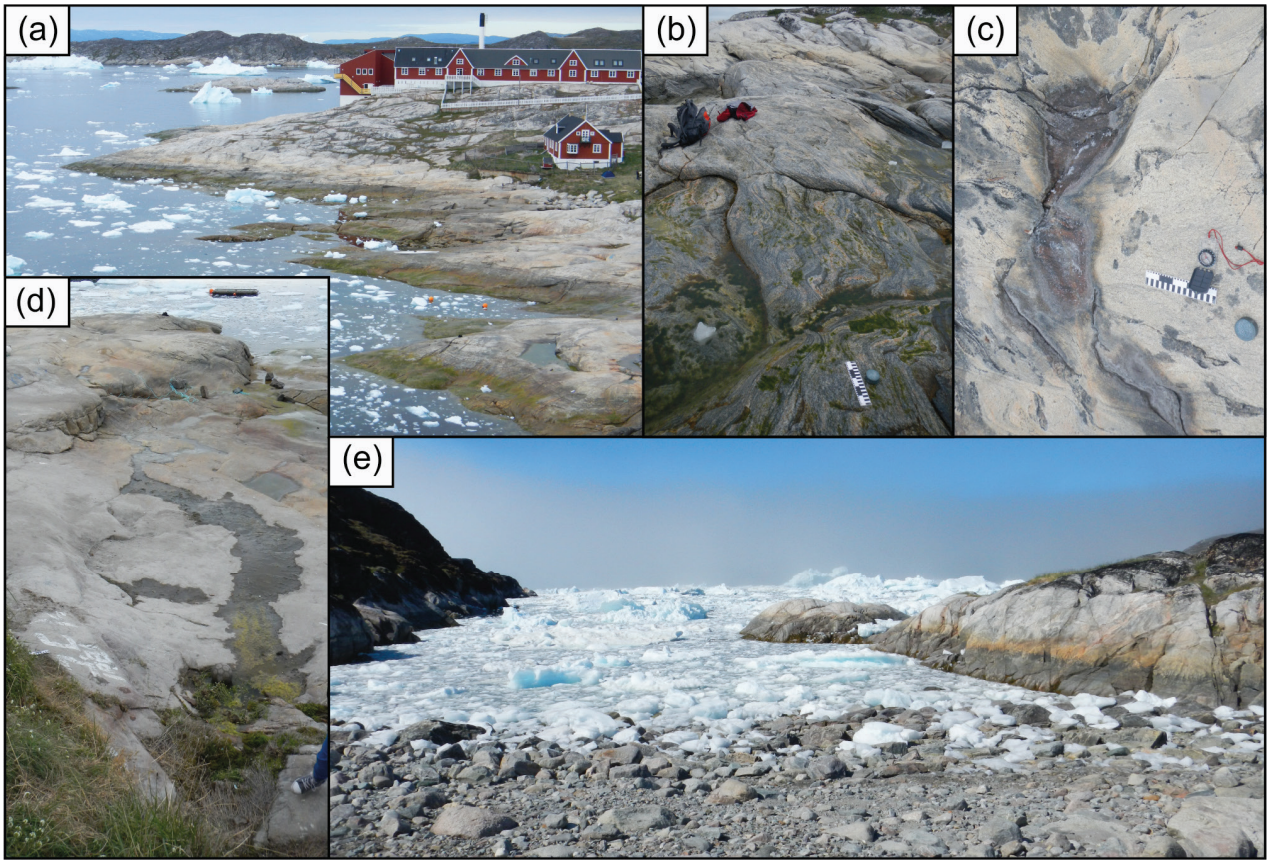

Fig. 3 (a) Zion Church Bay in Ilulissat. (b) Local accumulation of mafic minerals exposed on the rocky shore surface. (c) Weathering pits filled with salt crystals. (d) Groundwater released from the tundra running down to lower sections of the rocky coast. (e) One of the bays in Jakobshavn Isfjord filled with ice mélange. Note the yellowish colour of the rock surface on the right, similar to that in Zion Church Bay. (Photos: M. Strzelecki, 2013.)

Citation: *Polar Research* 2026, *45*, 12395, http://dx.doi.org/10.33265/polar.v45.12395

produced by Jakobshavn Isbræ may reach the height of 900 m (Lüthi et al. 2009), they usually don't reach our study area at this size. Most icebergs are much smaller. Video material suggests that such waves can be considerable in height and strength (e.g., https://www.youtube.com/watch?v=zlqY9fcYNX4).

There is no systematic, continuous monitoring programme for these specific waves, so their precise frequency has not been statistically established. Their occurrence is known to be highly variable and is directly linked to the intensity of iceberg calving. Based on field team observations, available videos and anecdotal accounts from local operators, periods of high calving activity can generate several roll waves per day. Periods of iceberg quiescence can last several days, with no significant waves reported. Our personal observations, accounts by other observers and videos suggest that the maximum wave run-up from these events is about 5 m.

The region's geological bedrock is primarily composed of metamorphic rocks belonging to the Nagssugtoqidian Orogen, which are part of the hard and resistant Precambrian Shield of West Greenland (St-Onge et al. 2009). The main rock type is Archaean orthogneiss, mainly granodioritic to tonalitic with biotite and/or hornblende (Henriksen et al. 2009; Kokfelt et al. 2023; Fig 3). It should be noted that only light grey massive and homogenous tonalite gneisses with the indicators of weak migmatization were found in the study area (Garde et al. 2002).

Seven longitudinal profiles (A–G) were conducted along a 500-m stretch of the coast (Fig. 2). These extended from the shoreline up to 60 m inland. Four coastal zones can be visually distinguished (Fig. 4). The observed colour variations reflect the distinct processes acting within each zone, rather than serving as the primary criterion for their classification.

Zone I corresponds to the rock surface between the mean low tide level and the lowest tidal reach and is regularly submerged during high tides. It is fully exposed only at the lowest tides and experiences the most frequent and prolonged seawater contact.

Zone II is defined as the mid-to-upper intertidal zone, extending from mean low tide to mean high tide. It is periodically submerged and exposed with the tidal cycle and shows evidence of biological colonization—by barnacles and algae, for example—typical of intertidal environments.

Zone III lies above the mean high tide level, beyond the reach of typical tidal inundation, but is periodically wetted by larger waves, including iceberg-roll-generated waves, and sea spray. This zone is characterized by a distinct yellowish rock surface colour, likely due to mineral or salt weathering.

Zone IV is located above the reach of both tidal waters and iceberg activity and serves as a geological background control. It shows no signs of direct marine influence (except for the influence of sea aerosols) and represents the natural weathering state of the rock in a fully terrestrial setting.

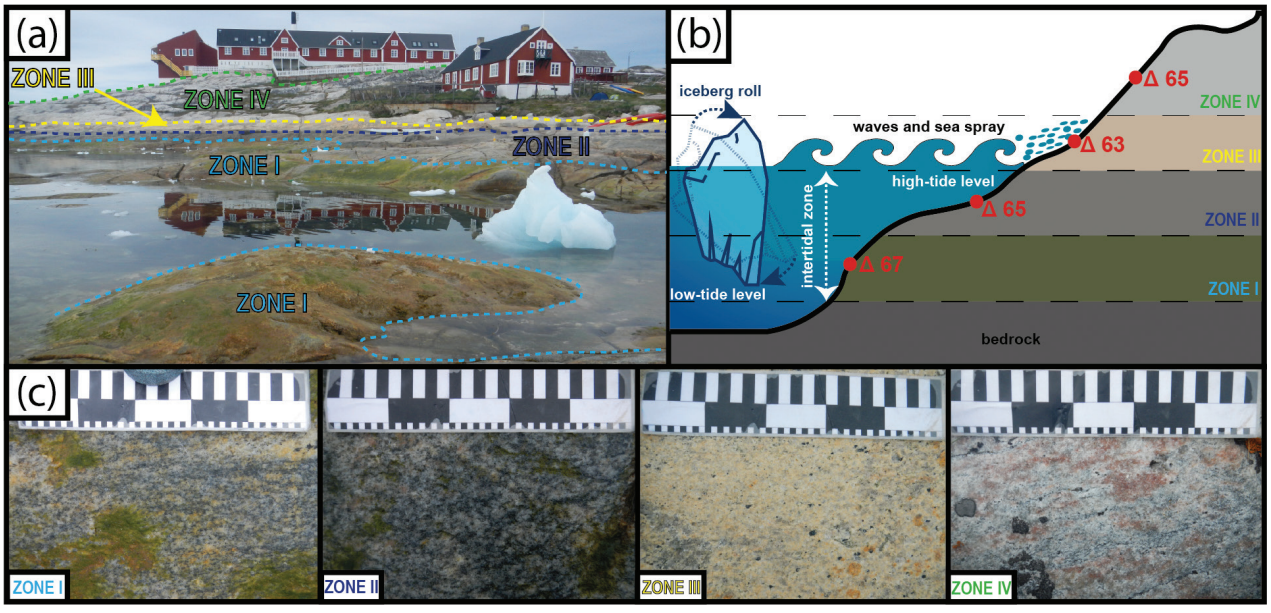

Fig. 4 (a) The zones in Zion Church Bay, viewed from the south. (b) Scheme of the zones, including the tide levels and mean resistance (R value) of each zone. (c) Typical structure of rock in each zone (the measuring tape is 10 cm long). Note the difference in colours, especially the characteristic yellow colouring in Zone III. (Photos: M. Strzelecki, 2013.)

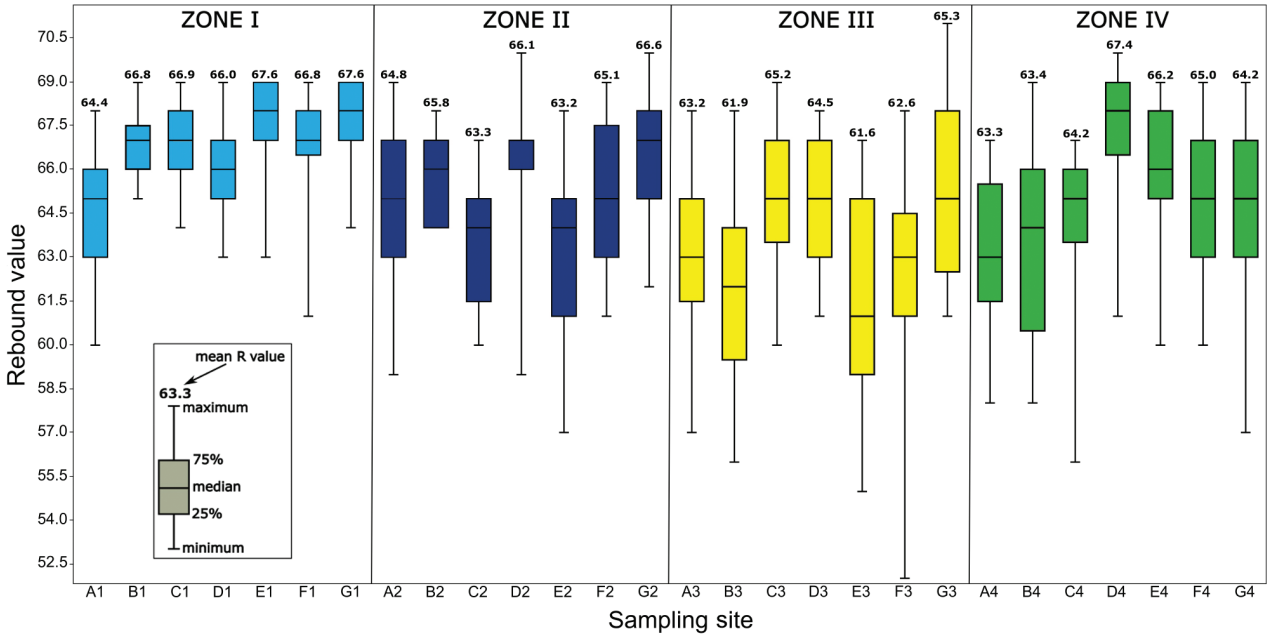

Fig. 5 Schmidt hammer measurements of rock surface resistance, that is, rebound values (*R* values) for each sampling site. Each site is identified by its profile letter and zone number.

Methodology

The degree of rock surface weathering was assessed using a Schmidt hammer, a common method for in situ measurements of rock properties (Goudie 2006). Previous studies using this method have described rock resistance in Arctic and Antarctic regions, including coastal and near-coastal zones, contributing to a better understanding of geomorphological changes in these harsh environments (Strzelecki 2011, 2017; Strzelecki et al. 2017; Migoń & Strzelecki 2024). Rock hardness is indicated by the rebound distance (R value) of a piston struck against the tested rock surface. Progressive weathering reduces rock cohesion and creates microfractures, which decrease the rock's ability to resist impact, resulting in lower rebound values. The survey data were collected during a dry Arctic summer day on 11 July 2013. Before each test, dirt was brushed off the rock surface and 25 blows were made in random places in a 10 × 10 cm square, as recommended by Niedzielski et al. (2009). The estimated resistance value at the sampling site is the mean of these 25 measurements. Sampling sites were grouped by coastal zones (Fig. 4). In each profile, a rock strength test was carried out in each zone, giving 28 sampling sites. Results for every sampling site were illustrated by mean values, standard errors at 95% confidence interval and minimum, maximum and median values (Table 2).

Paired *t*-tests were conducted six times to check if two zones had statistically significant differences in rock strength: zones 1 and 2, 1 and 3, 1 and 4, 2 and 3, 2 and 4 and 3 and 4). *T*-statistics were calculated in Microsoft Excel (T.TEST function, two-tailed distribution, paired *t*-test type), using the formula

$$t = \frac{\overline{d}}{\frac{s_d}{\sqrt{n}}},$$

where $\overline{d}$ is the mean of the differences between the average values at paired sampling sites, s_d is the sample standard deviation of the differences, and n is the number of pairs (in this study always 7). Values from the same transect were paired, for example, spot A1 (average value for Zone I, transect A) with spot A2 (average value for Zone II, transect A).

Results and discussion

The results of the Schmidt hammer tests were averaged (Figs. 4, 5, Table 1). The highest and most consistent (least error) R values (mean 67) were recorded in the low tide zone (Zone I), while the lowest rebound values (mean 63) occurred in the characteristic yellowish zone (Zone III). Zones with similar results are the high-tide zone (Zone II) and the zone not affected by waves and tides (Zone IV).

Citation: *Polar Research* 2026, *45*, 12395, http://dx.doi.org/10.33265/polar.v45.12395

Table 1 Mean rock surface resistance differences between zones with results of the paired *t*-test.

Zone	Zone II	Zone III	Zone IV
Zone I	+1.611 (p = 0.0532)[a]	+3.143 (p = 0.0048)[c]	+1.811 (p = 0.0308)[b]
Zone II		+1.531 (p = 0.569)[a]	+0.200 (p = 0.8036)
Zone III			-1.331 (p = 0.1509)

[a]Significant at 10%. [b]Significant at 5%. [c]Significant at 1%.

There are statistically significant differences in rock resistance between Zone I and all other zones and between Zones II and III (Table 1). No significant difference between the other pairs of zones was detected—either there was no difference or seven transects are not enough to show a difference that may really exist.

Zone I: low intertidal zone

Zone I is defined by the near-constant presence of seawater. The rock surface is only exposed to subaerial conditions during very low tides, as the marine vegetation colonizing these rocks shows (Fig. 4). This zone is characterized by significantly higher R values than all other zones (Fig. 5). Two key factors may explain this.

First, this zone is subjected to regular scouring by tidal action and the abrasive movement of sea ice during winter. These dynamic processes can remove weathered material from the rock surface, resulting in relatively higher rock resistance, as demonstrated in other studies (e.g., Williams & Robinson 1983; Blanco-Chao et al. 2007; Fig. 4; Table 2). Despite the presence of algae, which typically require stable surfaces for colonization, this biological growth is likely confined to microenvironments that are temporarily sheltered or rapidly recolonized between disturbance events such as winter ice scouring.

Second, Zone I is exposed to more stable thermal conditions due to frequent submersion in seawater, which buffers short or long-term temperature extremes. While not entirely constant, seawater temperatures fluctuate less than air temperatures, reducing the frequency of freeze–thaw cycles that mainly enhance frost weathering. Similar results can be found at the rocky coasts of Svalbard, where the intertidal zone was found to have the highest rock resistance (Strzelecki et al. 2017).

In general, this zone is simply exposed to subaerial conditions for a shorter duration than higher zones and may therefore experience less intense thermal stress.

Table 2 Statistical parameters of Schmidt hammer rock tests for each of the sampling sites and for particular zones.

Sampling site	Mean R value	Standard error (95% CI[a])	Min.	Max.	Median
A1	64.4	0.86	60	68	65
B1	66.8	0.42	65	69	67
C1	66.9	0.54	64	69	67
D1	66.0	0.59	63	69	66
E1	67.6	0.59	63	69	68
F1	66.8	0.76	61	69	67
G1	67.6	0.52	64	69	68
Zone I	66.6	0.82			
A2	64.8	1.10	59	69	65
B2	65.8	0.53	64	68	66
C2	63.3	0.80	60	67	64
D2	66.1	0.94	59	70	67
E2	63.2	1.20	57	68	64
F2	65.1	0.97	61	69	65
G2	66.6	0.79	62	70	67
Zone II	65.0	0.98			
A3	63.2	0.94	57	68	63
B3	61.9	1.13	56	68	62
C3	65.2	0.99	60	69	65
D3	64.5	0.87	61	68	65
E3	61.6	1.34	55	67	61
F3	62.6	1.37	52	68	63
G3	65.3	1.22	61	71	65
Zone III	63.5	1.14			
A4	63.3	1.06	58	67	63
B4	63.4	1.10	58	69	64
C4	64.2	0.98	56	67	65
D4	67.4	0.78	61	70	68
E4	66.2	0.91	60	69	66
F4	65.0	0.96	60	69	65
G4	64.2	1.34	57	69	65
Zone IV	64.8	1.13			

[a]Confidence interval.

Zone II: mid–upper intertidal zone

This zone is located in the intertidal zone, where rock is in regular contact with water (Fig. 4). The rock surface here is exposed to the air during each tidal cycle. It is characterized by significantly lower R values than Zone I (Table 1). The relatively effective thermal abrasion in this zone appears to be linked to frequent freeze–thaw cycles, which are commonly observed in similar environments, such as the shores of Svalbard (Prick 2003; Strzelecki 2017). Thermal abrasion may also occur in other zones; however, its intensity seems to be higher in the intertidal zone because of regular wetting and daily temperature fluctuations. In addition, icefoot activity during winter likely contributes to rock surface erosion.

As the ice forms and shifts, it may scratch against the substrate, enhancing surface wear (e.g., Nielsen 1979; Dionne & Brodeur 1988). This zone may therefore experience a combination of thermal and mechanical erosion more intensely than the others. Although icefoot activity can contribute to the removal of weathered material and expose fresher, potentially more resistant, rock surfaces, the results of this study suggest a net decrease in surface strength. This apparent contradiction may be explained by the combined mechanical impact of ice scouring and the concurrent action of freeze–thaw weathering, which together can progressively weaken the rock substrate despite the removal of superficial weathered layers.

The significantly lower resistance values recorded in profiles C and E appear to be associated with local accumulations of mafic minerals, which are more susceptible to weathering (Figs. 3, 4). Mafic mineral deposits were not observed to the same extent in other profiles, which may explain local variations in R values.

Zone III: supratidal wash zone

This zone is above the tidal range and is only in contact with seawater as a result of wave run-up and sea spray (Fig. 4). In this zone, the rock surface also becomes wet during precipitation and snowmelt. It is characterized by a yellowish-brown coating on the rock surface not associated with lichens (Fig. 4). The rocks in our study area were mainly covered by well-developed black and green lichens. Drawing from the literature, we suggest that this iron-staining colouration is derived from the oxidation of iron-bearing minerals in the rock outcrop. This phenomenon was observed by Tarr (1897) in western Greenland and Baffin Island and later noted by Jahn & Manecki (1991) along other segments of the coastline belonging to the Nagssugtoqidian orogen (Fig. 3). Recent studies suggest that mineral oxidation processes result in the formation of rock varnish exhibiting this colouration (Dorn & Krinsley 2019).

Rock surface resistance is particularly low here—statistically significantly lower than in Zone I and Zone II (Fig. 4, Table 1). Increased weathering may be driven by many factors. The most important of these are discussed in a later section.

Zone IV: terrestrial weathering zone

This zone is high above the shoreline (ca. 8–9 m), where seawater does not affect the rock surface directly (Figs. 4, 5). However, it is likely that the rock surface may be affected by airborne marine aerosols (e.g., Senderak & Wąsowski 2016). The rock surface is statistically significantly weaker than in Zone I (Table 1). These lower values may be related to the longer exposure to weathering processes and biological weathering resulting from the presence of lichens (Figs. 4, 5; e.g., Jie & Blume 2002). In addition, snow drifts can form in winter, protecting this part of the coastal platform from denudation processes. Here, where waves cannot reach the rock surface, weathering is controlled by periglacial processes such as frost weathering and thermal cracking.

Possible causes of reduced rock resistance in Zone III: supratidal wash zone

We suspect that the impact of iceberg-roll waves that are capable of wetting this zone may be one of the key drivers of rock surface weakening. The bay lies directly in the path of numerous icebergs calving from Jakobshavn Isfjord. Icebergs can dampen the impact of wind waves and storms (Bendixen & Kroon 2017). However, when they rotate, they can generate powerful waves capable not only of eroding the entire intertidal zone but also of removing surface material from areas located several metres above the current sea level. Multiple videos of the Ilulissat coast present evidence of iceberg-roll-generated waves running up local rocky shores. We propose that iceberg-roll-generated waves are the most likely events delivering ice fragments above the high-water line that may scour the rock surface. This process could contribute to the initial physical damage of exposed rock surfaces, enhancing their susceptibility to subsequent weathering. In addition to direct abrasion by ice fragments, these episodic waves also periodically wet the rock surface above the normal tidal limit, which promotes both physical and chemical weathering processes. During freeze–thaw cycles, the expansion of water in microscopic pores leads to the deeper penetration of moisture and oxygen into the rock, accelerating its chemical weathering.

Given that no other high-energy wave processes, such as landslide or earthquake tsunamis, are known to affect this part of the coast, iceberg-roll-generated waves appear to be the only plausible agent capable of generating such mechanical impacts.

In addition, the surface of the rock may be affected by chemical weathering caused by salt. In some places on the rock surface analysed in this work, we observed weathering pits filled with salt crystals (Fig. 3), similar to those described in the Canadian Arctic (Watts 1983). Although salt crystallization processes are typically most active under alternating wetting and drying conditions, field observations suggest that such cycles can occur during summer, when rock surfaces periodically dry

Citation: *Polar Research* 2026, *45*, 12395, http://dx.doi.org/10.33265/polar.v45.12395

between rainfall, sea-spray events and insolation. This promotes repeated cycles of salt crystallization and hydration, consistent with the mechanisms described by Cooke & Smalley (1968), as evidenced by the presence of salt efflorescence on exposed surfaces (Fig. 3). Scientists studying weathering pits on the coasts of the Cumberland Peninsula, on Baffin Island, have noted accelerated, salt-influenced weathering in similar type of bedrock (e.g., Dyke 1977; Birkeland 1978). In this area, the salts responsible for these effects are primarily derived from sea spray.

In addition to the processes mentioned above, the following processes can reduce rock resistance.

First, sea spray wets the rock surface as a less intensive, but more continuous, source of moisture and salt than waves and may have a similar impact on the rock strength.

Second, as a result of the retreat of the Greenland ice sheet, the study area is subject to isostatic uplift, which has been estimated at 1.6 mm yr^{-1} in Ilulissat (Dietrich et al. 2005). At this rate, the area rises by about 16 cm per century, indicating that rocks in Zone IV (higher elevated) have been exposed for many centuries, whereas Zone III (8–9 m above present sea level) was exposed relatively more recently. The spatial extent of this process depends on local topography and coastal slope, with low-lying areas becoming exposed first; in these locations, the characteristic colouration is particularly evident. Rock surfaces that were previously unexposed to subaerial conditions are now subjected to both physical and chemical weathering. Chemical weathering contributes to the oxidation of iron-bearing minerals and the development of characteristic colouration, while physical weathering leads to cracking and rock fragmentation. The importance of this process is highlighted by the difference between Zones III and IV, where Zone IV shows little visible colouration despite its longer exposure, likely because of the reduced influence of wet–dry cycles. In this context, more detailed studies could be conducted, including analyses of rock chemical composition and examinations of their microstructure, to better understand how exposure due to uplift affects coastal rock weathering.

Third, chemical compounds transported from higher tundra areas by precipitation can react with the rock surface, gradually altering mineral composition and reducing mechanical strength (Fig. 3). In addition, bioagents such as lichens and microbes play a significant role in shaping rocky cliffs and platforms in cold regions (Strzelecki 2017). These organisms can both physically disrupt rock surfaces and produce chemical agents, amplifying the weathering process and further weakening rocks.

Fourth, the formation of the icefoot during winter introduces processes that can influence rock surfaces in cold coastal regions. However, in our study site, the icefoot is formed in a platform area lacking free sediment, severely limiting the erosion the icefoot can cause. On the other hand, the ice foot may have a protective role. Especially in winter, together with snow, the icefoot provides a natural protection against the action of waves, currents, tides, other physical processes and organic processes (Dionne 1973). It is likely that the processes reducing rock resistance in this zone occur mainly in summer, as the weathered surface is preserved in winter. During winter, the coasts are partially separated from the direct action of shaping factors, and the evolution of the coastlines in cold regions is relatively slow (Dionne 1973).

The weathering patterns and discolouration observed in Zone III result from the interplay of multiple processes, both mechanical and chemical, particularly the oxidation of ferrous minerals. It is difficult to identify a single dominant cause. Observations from Zion Church Bay suggest that chemical weathering plays the primary role in shaping the surface alterations. This does not exclude the influence of physical processes, particularly the supply of seawater in the form of waves generated by drifting icebergs, which may enhance both chemical and mechanical weathering. In particular, this affects wet–dry and freeze–thaw cycles at the rock surface. Overall, the synergistic action of physical and chemical processes appears to control the degree of rock weakening in this zone.

Conclusions

This study provides clear evidence that our understanding of rocky coast weathering in still-glaciated parts of the Arctic is incomplete. Through observations from a small rocky cove in western Greenland, we detected a conspicuous reduction in rock surface resistance above the high-tide level. This finding suggests the presence of supplementary forces that regulate weathering processes, extending beyond the action of waves caused by wind and the tides. We postulate that this reduction is caused by the impact of iceberg-roll-generated waves—a phenomenon unique to cold regions where marine-terminating glaciers still dominate the coastal landscape. These waves, in conjunction with sea spray, subject the coastal rocks to intense physical pressure, while chemical and biological agents exploit these weaknesses.

As the cryosphere undergoes degradation, there will be an intensification of energy fluxes at the glacier–ocean interface. This will result in a change to the mechanisms controlling the development of cold-region coastal systems. A comprehensive understanding of the coastal

hazards associated with iceberg-roll-generated waves is needed in order to assess the future stability of Arctic shores and the safety of the populations that inhabit them.

Acknowledgements

The authors wish to express their gratitude to Piotr Migoń and Ronald Dorn for their insights into rock weathering in cold environments. We also appreciate the critical review and editorial support provided by Robert Spielhagen and the anonymous reviewers. MCS designed the study, obtained funding for it and collected field data. Analyses were performed by OK and MS. KS supported lithological analyses. The original draft was written by OK, and all authors contributed to the final manuscript through multiple rounds of revision.

Disclosure statement

The authors report no conflict of interest.

Funding

This research was financed by the National Science Centre in Poland through funding to MCS for the project Paraglacial Coasts Transformed by Tsunami Waves—Past, Present and Warmer Future (GLAVE, UMO 2020/38/E/ST10/00042) obtained by MCS.

Data availability

Our data set of Schmidt hammer measurements in Zion Church Bay, Greenland, is stored at the Polish Polar Database and is accessible here: https://polar.cenagis.edu.pl/dataset/schmidt-hammer-measurments-in-zion-church-bay-western-greenland.

References

Aga J., Piermattei L., Girod L., Aalstad K., Eiken T., Kääb A. & Westermann S. 2024. Acceleration of coastal-retreat rates for High-Arctic rock cliffs on Brøggerhalvøya, Svalbard, over the past decade. *Earth Surface Dynamics 12*, 1049–1070, doi: 10.5194/esurf-12-1049-2024.

Amundson J.M., Truffer M., Lüthi M.P., Fahnestock M., West M. & Motyka R.J. 2008. Glacier, fjord, and seismic response to recent large calving events, Jakobshavn Isbræ, Greenland. *Geophysical Research Letters 35*, L22501, doi: 10.1029/2008GL035281.

Bendixen M. & Kroon A. 2017. Conceptualizing delta forms and processes in Arctic coastal environments. *Earth Surface Processes and Landforms 42*, 1227–1237, doi: 10.1002/esp.4097.

Bendixen M., Lønsmann Iversen L., Anker Bjørk A., Elberling B., Westergaard-Nielsen A., Overeem I., Barnhart K.R., Abbas Khan S., Box J.E., Abermann J., Langley K. & Kroon A. 2017. Delta progradation in Greenland driven by increasing glacial mass loss. *Nature 550*, 101–104, doi: 10.1038/nature23873.

Birkeland P.W. 1978. Soil development as an indication of relative age of Quaternary deposits, Baffin Island, N.W.T., Canada. *Arctic and Alpine Research 10*, 733–747, doi: 10.1080/00040851.1978.12004011.

Blanco-Chao R., Pérez-Alberti A., Trenhaile A.S., Costa-Casais M. & Valcárcel-Díaz M. 2007. Shore platform abrasion in a para-periglacial environment, Galicia, northwestern Spain. *Geomorphology 83*, 136–151, doi: 10.1016/j.geomorph.2006.06.028.

Buchwał A., Szczuciński W., Strzelecki M.C. & Long A.J. 2015. New insights into the 21 November 2000 tsunami in west Greenland from analyses of the tree-ring structure of *Salix glauca*. *Polish Polar Research 36*, 51–65, doi: 10.1515/popore-2015-0005.

Cooke R.U. & Smalley I.J. 1968. Salt weathering in desert. *Nature 217*, 1226–1227, doi: 10.1016/S0016-7878(81)80015-6.

Dawson A.G., Matthews J.A. & Shakesby R.A. 1987. Rock platform erosion on periglacial shores: a modern analogue for Pleistocene rock platforms in Britain. In J. Boardman (ed.): *Periglacial processes and landforms in Britain and Ireland*. Pp. 173–182. Cambridge: Cambridge University Press.

Dietrich R., Maas H.G., Baessler M., Rülke A., Richter A., Schwalbe E. & Westfeld P. 2007. Jakobshavn Isbræ, west Greenland: flow velocities and tidal interaction of the front area from 2004 field observations. *Journal of Geophysical Research—Earth Surface 112*, F03S21, doi: 10.1029/2006JF000601.

Dietrich R., Rülke A. & Scheinert M. 2005. Present-day vertical crustal deformations in west Greenland from repeated GPS observations. *Geophysical Journal International 163*, 865–874, doi: 10.1111/j.1365-246X.2005.02766.x.

Dionne J.C. 1973. La notion de pied de glace (icefoot), en particulier dans l'estuaire du Saint-Laurent. (The concept of the ice foot, particularly in the St. Lawrence estuary.) *Cahiers de Géographie du Québec 17*, 221–250, doi: 10.7202/021116ar.

Dionne J.C. & Brodeur D. 1988. Frost weathering and ice action in shore platform development, with particular reference to Quebec, Canada. *Zeitschrift für Geomorphologie Supplementband 71*, 117–130.

Dorn R.I. & Krinsley D.H. 2019. Nanoscale observations support the importance of chemical processes in rock decay and rock coating development in cold climates. *Geosciences 9*, article no. 121, doi: 10.3390/geosciences9030121.

Dyke A.S. 1977. *Quaternary geomorphology, glacial chronology, and climatic and sea-level history of the southwestern Cumberland Peninsula, Baffin Island, Northwest Territories, Canada*. PhD thesis, University of Colorado, Boulder.

Forman S.L., Lubinski D.J., Ingólfsson Ó., Zeeberg J.J., Snyder J.A., Siegert M.J. & Matishov G.G. 2004. A review of postglacial emergence on Svalbard, Franz

Josef Land and Novaya Zemlya, northern Eurasia. *Quaternary Science Reviews 23*, 1391–1434, doi: 10.1016/j.quascirev.2003.12.007.

Garde A.A., Connelly J.N., Krawiec A.W., Piazolo S. & Thrane K. 2002. A coastal survey in the southern part of the Palaeoproterozoic Rinkian fold belt, central West Greenland. *Geology of Greenland Survey Bulletin 191*, 33–38, doi: 10.34194/ggub.v191.5109.

Goudie A.S. 2006. The Schmidt hammer in geomorphological research. *Progress in Physical Geography 30*, 703–718, doi: 10.1177/0309133306071954.

Henriksen N., Higgins A.K., Kalsbeek F. & Pulvertaft T.C.R. 2009. *Greenland from Archaean to Quaternary. Descriptive text to the 1995 Geological map of Greenland, 1:2500 000. 2nd edition. Geological Survey of Denmark and Greenland Bulletin 18*. Copenhagen: Geological Survey of Denmark and Greenland Ministry of Climate and Energy.

Higman B., Shugar D.H., Stark C.P., Ekström G., Koppes M.N., Lynett P., Dufresne A., Haeussler P.J., Geertsema M., Gulick S., Mattox A., Venditti J.G., Walton M.A.L., McCall N., McKittrick E., MacInnes B., Bilderback E.L., Tang H., Willis M.J. & Loso M. 2018. The 2015 landslide and tsunami in Taan Fiord, Alaska. *Scientific Reports 8*, article no. 12993, doi: 10.1038/s41598-018-30475-w.

Irrgang A.M., Bendixen M., Farquharson L.M., Baranskaya A.V., Erikson L.H., Gibbs A.E., Ogorodov S.A., Overduin P.P., Lantuit H., Grigoriev M.N. & Jones B.M. 2022. Drivers, dynamics and impacts of changing Arctic coasts. *Nature Reviews Earth and Environment 3*, 39–54, doi: 10.1038/s43017-021-00232-1.

Jahn A. & Manecki A. 1991. Rock varnish coat on cobbles in Hornsund area, Spitsbergen. *Polish Polar Research 12*, 279–288.

Jie C. & Blume H.P. 2002. Rock-weathering by lichens in Antarctic: patterns and mechanisms. *Journal of Geographical Sciences 12*, 387–396, doi: 10.1007/BF02844595.

Joughin I., Abdalati W. & Fahnestock M. 2004. Large fluctuations in speed on Greenland's Jakobshavn Isbræ glacier. *Nature 432*, 608–610, doi: 10.1038/nature03130.

Kasprzak M., Strzelecki M.C., Traczyk A., Kondracka M., Lim M. & Migała K. 2017. On the potential for a bottom active layer below coastal permafrost: the impact of seawater on permafrost degradation imaged by electrical resistivity tomography (Hornsund, SW Spitsbergen). *Geomorphology 293*, 347–359, doi: 10.1016/j.geomorph.2016.06.013.

Kavan J. & Strzelecki M.C. 2023. Glacier decay boosts the formation of new Arctic coastal environments—perspectives from Svalbard. *Land Degradation & Development 34*, 3467–3474, doi: 10.1002/ldr.4695.

Kokfelt T.F., Willerslev E., Bjerager M., Heijboer T., Keulen N., Larsen L.M., Pedersen C.B., Pedersen M., Svennevig K., Sønderholm M., Walentin K.T. & Weng W.L. 2023. Seamless digital 1:500 000 scale geological map of Greenland, version 2.0. Copenhagen: Geological Survey of Denmark and Greenland, doi: 10.22008/FK2/FWX5ET.

Kostrzewa O., Szczypińska M., Kavan J., Senderak K., Novák M. & Strzelecki M.C. 2024. A boulder beach formed by waves from a calving glacier revisited: multidecadal tsunami-controlled coastal changes in front of Eqip Sermia, west Greenland. *Permafrost and Periglacial Processes 35*, 312–325, doi: 10.1002/ppp.2235.

Lantuit H., Overduin P.P., Couture N., Wetterich S., Aré F., Atkinson D., Brown J., Cherkashov G., Drozdov D., Forbes D.L., Graves-Gaylord A., Grigoriev M., Hubberten H.W., Jordan J., Jorgenson T., Ødegård R.S., Ogorodov S., Pollard W.H., Rachold V. & Vasiliev A. 2012. The Arctic Coastal Dynamics Database: a new classification scheme and statistics on Arctic permafrost coastlines. *Estuaries and Coasts 35*, 383–400, doi: 10.1007/s12237-010-9362-6.

Lim M., Strzelecki M.C., Kasprzak M., Świrad Z.M., Webster C., Woodward J. & Gjelten H. 2020. Arctic rock coast responses under a changing climate. *Remote Sensing of Environment 236*, article no. 111500, doi: 10.1016/j.rse.2019.111500.

Long A.J., Szczuciński W. & Lawrence T. 2015. Sedimentary evidence for a mid-Holocene iceberg-generated tsunami in a coastal lake, west Greenland. *Arktos 1*, article no. 6, doi: 10.1007/s41063-015-0007-7.

Lüthi M.P., Fahnestock M. & Truffer M. 2009. Calving icebergs indicate a thick layer of temperate ice at the base of Jakobshavn Isbræ, Greenland. *Journal of Glaciology 55*, 563–566, doi: 10.3189/002214309788816650.

MacAyeal D.R., Abbot D.S. & Sergienko O.V. 2011. Iceberg-capsize tsunamigenesis. *Annals of Glaciology 52*, 51–56, doi: 10.3189/172756411797252103.

MacAyeal D.R., Okal E.A., Aster R.C. & Bassis J.N. 2009. Seismic observations of glaciogenic ocean waves (micro-tsunamis) on icebergs and ice shelves. *Journal of Glaciology 55*, 193–206, doi: 10.3189/002214309788608679.

Migoń P. & Strzelecki M.C. 2024. Outcrops of columnar andesite shaped by periglacial processes—Jersak Hills, King George Island, Antarctica. *Quaestiones Geographicae 43*, 5–16, doi: 10.14746/quageo-2024-0031.

Møller E.F., Christensen A., Larsen J., Mankoff K.D., Ribergaard M.H., Sejr M., Wallhead P. & Maar M. 2023. The sensitivity of primary productivity in Disko Bay, a coastal Arctic ecosystem, to changes in freshwater discharge and sea ice cover. *Ocean Science 19*, 403–420, doi: 10.5194/os-19-403-2023.

Niedzielski T., Migoń P. & Placek A. 2009. A minimum sample size required from Schmidt hammer measurements. *Earth Surface Processes and Landforms 34*, 1713–1725, doi: 10.1002/esp.1851.

Nielsen N. 1979. Ice-foot processes: observations of erosion of the rocky coast, Disko, west Greenland. *Zeitschrift für Geomorphologie 23*, 321–331, doi: 10.1127/zfg/23/1979/321.

Nielsen N. 1992. A boulder beach formed by waves from a calving glacier; Eqip Sermia, west Greenland. *Boreas 21*, 159–168, doi: 10.1111/j.1502-3885.1992.tb00023.x.

Prick A. 2003. Frost weathering and rock fall in an Arctic environment, Longyerbyen, Svalbard. In M. Phillips et al. (eds.): *Permafrost: proceedings of the Eight International Conference on Permafrost, 21–25 July, Zürich, Switzerland. Vol. 2.* Pp. 907–912. Lisse: A.A. Balkema.

Ribeiro S., Moros M., Ellegaard M. & Kuijpers A. 2012. Climate variability in west Greenland during the past 1500 years: evidence from a high-resolution marine

palynological record from Disko Bay. *Boreas 41*, 68–83, doi: 10.1111/j.1502-3885.2011.00216.x.

Senderak K. & Wąsowski K. 2016. Chemical weathering of talus slopes: the example of slopes in the Brattegg Valley, SW Spitsbergen. *Studia Geomorphologica Carpatho-Balcanica 50*, 105–122.

Shakesby R.A., Shakesby J.A.M., Matthews R.A. & Shakesby R.A. 1987. Frost weathering and rock platform erosion on periglacial lake shorelines: a test of a hypothesis. *Norsk Geologisk Tidsskrift 67*, 197–203.

St-Onge M.R., Van Gool J.A.M., Garde A.A. & Scott D.J. 2009. Correlation of Archaean and Palaeoproterozoic units between northeastern Canada and western Greenland. *Geological Society Special Publication 318*, 193–235, doi: 10.1144/SP318.7.

Strzelecki M.C. 2011. Schmidt hammer tests across a recently deglacierized rocky coastal zone in Spitsbergen—is there a coastal amplification of rock weathering in polar climates? *Polish Polar Research 32*, 239–252, doi: 10.2478/v10183-011-0017-5.

Strzelecki M.C. 2017. The variability and controls of rock strength along rocky coasts of central Spitsbergen, High Arctic. *Geomorphology 293*, 321–330, doi: 10.1016/j.geomorph.2016.06.014.

Strzelecki M.C. & Jaskólski M.W. 2020. Arctic tsunamis threaten coastal landscapes and communities—survey of Karrat Isfjord 2017 tsunami effects in Nuugaatsiaq, western Greenland. *Natural Hazards and Earth System Sciences 20*, 2521–2534, doi: 10.5194/nhess-20-2521-2020.

Strzelecki M.C., Kasprzak M., Lim M., Świrad Z.M., Jaskólski M., Pawłowski Ł. & Modzel P. 2017. Cryo-conditioned rocky coast systems: a case study from Wilczekodden, Svalbard. *Science of the Total Environment 607/608*, 443–453, doi: 10.1016/j.scitotenv.2017.07.009.

Strzelecki M.C., Long A.J., Lloyd J.M., Małecki J., Zagórski P., Pawłowski Ł. & Jaskólski M.W. 2018. The role of rapid glacier retreat and landscape transformation in controlling the post–Little Ice Age evolution of paraglacial coasts in central Spitsbergen, Billefjorden, Svalbard. *Land Degradation and Development 29*, 1962–1978, doi: 10.1002/ldr.2923.

Strzelecki M.C., Szczuciński W., Dominiczak A., Zagórski P., Dudek J. & Knight J. 2020. New fjords, new coasts, new landscapes: the geomorphology of paraglacial coasts formed after recent glacier retreat in Brepollen (Hornsund, southern Svalbard). *Earth Surface Processes and Landforms 45*, 1325–1334, doi: 10.1002/esp.4819.

Svennevig K., Hicks S.P., Forbriger T., Lecocq T., Widmer-Schnidrig R., Mangeney A., Hibert C., Korsgaard N.J., Lucas A., Satriano C., Anthony R.A., Mordret A., Schippkus S., Rysgaard S., Boone W., Gibbons S.J., Cook K.L., Glimsdal S., Løvholt F., Van Noten K., Assink J.D., Marboeuf A., Lomax A., Vanneste K., Taira T., Spagnolo M., De Plaen R., Koelemeijer P., Ebeling C., Cannata A., Harcourt W.D., Cornwell D.G., Caudron C., Poli P., Bernard P., Larose E., Stutzmann E., Voss P.H., Lund B., Cannavo F., Castro-Díaz M.J., Chaves E., Dahl-Jensen T., De Pinho Dias N., Déprez A., Develter R., Dreger D., Evers L.G., Fernández-Nieto E.D., Ferreira A.M.G., Funning G., Gabriel A.A., Hendrickx M., Kafka A.L., Keiding M., Kerby J., Khan S.A., Dideriksen A.K., Lamb O.D., Larsen T.B., Lipovsky B., Magdalena I., Malet J.P., Myrup M., Rivera L., Ruiz-Castillo E., Wetter S. & Wirtz B. 2024. A rockslide-generated tsunami in a Greenland fjord rang Earth for 9 days. *Science 385*, 1196–1205, doi: 10.1126/science.adm9247.

Svennevig K., Keiding M., Korsgaard N.J., Lucas A., Owen M., Poulsen M.D., Priebe J., Sørensen E.V. & Morino C. 2023. Uncovering a 70-year-old permafrost degradation-induced disaster in the Arctic: the 1952 Niiortuut landslide-tsunami in central west Greenland. *Science of the Total Environment 859*, article no. 160110, doi: 10.1016/j.scitotenv.2022.160110.

Tarr R.S. 1897. Rapidity of weathering and stream erosion in the Arctic latitudes. *American Geologist 19*, 131–136.

Trenhaile A.S. & Mercan D.W. 1984. Frost weathering and the saturation of coastal rocks. *Earth Surface Processes and Landforms 9*, 321–331, doi: 10.1002/esp.3290090405.

Watts S.H. 1983. Weathering processes and products under arid Arctic conditions. *Geografiska Annaler Series A 65*, 85–98, doi: 10.1080/04353676.1983.11880076.

Williams R.B.G. & Robinson D.A. 1983. The effect of surface texture on the determination of the surface hardness of rock using the Schmidt hammer. *Earth Surface Processes and Landforms 8*, 289–292, doi: 10.1002/esp.3290080311.

Wolper J., Gao M., Lüthi M.P., Heller V., Vieli A., Jiang C. & Gaume J. 2021. A glacier–ocean interaction model for tsunami genesis due to iceberg calving. *Communications Earth & Environment 2*, article no. 130, doi: 10.1038/s43247-021-00179-7.

Zagórski P., Jarosz K. & Superson J. 2020. Integrated assessment of shoreline change along the Calypsostranda (Svalbard) from remote sensing, field survey and GIS. *Marine Geodesy 43*, 433–471, doi: 10.1080/01490419.2020.1715516.